



CLINICAL ARTICLE

Surgical Tool Handle Vibration-Based Drilling State Recognition During Hip Fracture Fixation

Guangming Xia, PhD¹ , Wei Liu, MD^{2,4}, He Bai, MD², Yuan Xue, PhD² , Yu Dai, PhD¹, Ping Lei, MD³, Jianxun Zhang, PhD¹

¹Institute of Robotics and Automatic Information System, Department of ²Orthopedic Surgery and ³Geriatrics, Tianjin Medical University General Hospital and ⁴Department of Orthopaedic Surgery, Tianjin Baodi Hospital, Tianjin, China

Objectives: Traditional manual drilling during hip fracture fixation can easily lead to unstable fixation and vascular damage. This study aimed to investigate a safe and easy-to-use robot-assisted method to automatically drill bone and distinguish critical bone drilling states with high accuracy in real-time for the bone hole-making process during hip fracture fixation.

Methods: A bone-drilling robotic system was designed to automatically create holes in the femoral neck. Four fresh pig femurs were drilled at the posterosuperior femoral neck using three modes: “all-in” (AI), “in-out-in” (IOI), and “percutaneous fixation” (PF). A high-frequency accelerometer captured the generated vibrations of the drill handle, which were then transferred to a personal computer using a data acquisition card. Five bone drilling states are defined, including: “drill idling,” “initial drilling,” “in the cancellous bone,” “out the femoral neck,” and “in the cortical bone.” The harmonic distribution of the vibration signal was extracted by fast Fourier transform (FFT) and used as a critical feature to identify different drilling states. To prove the difference in the harmonic distribution at different drilling states, an independent sample *t*-test was used to compare the percentage of the first harmonic amplitude in the first 10 harmonics at each drilling state. A neural network classifier was trained with the frequency spectrum as the input and the drilled state as the output to distinguish the critical bone drilling states with high accuracy in real-time. The classifier was trained and tested on four specimens to ensure that the surgical robot could accurately identify the five drilling states.

Results: In each specimen, the harmonic distributions of the drilling vibration at different drilling modes were significantly different ($p < 0.05$). The average recognition accuracies of the drilling state for the four specimens were all higher than 84%. The three defined modes were distinguished with extremely high accuracies. The recognition accuracies of “in the cancellous bone” for specimens 1 to 4 were 83.2%, 84.8%, 92.9%, and 84.7%. The recognition accuracies of “in out the femoral neck” from specimens 1 to 4 are 98.2%, 88.4%, 95.8%, and 88.8%. The recognition accuracies of “in the cortical bone” for specimens 1 to 4 were 94.6%, 80.8%, 95.5%, and 85.8%.

Conclusions: The proposed robot-assisted method can automatically distinguish five critical bone-drilling states with high accuracy in real-time to avoid weak fixation and damage to the lateral epiphyseal artery.

Key words: Robot-assisted surgery; Hip fracture fixation; Bone drilling; Vibration signal processing; State estimation

Introduction

Hip fractures have a high incidence worldwide,¹ and the treatment choice for most hip fractures is operative,²

usually involving *in situ* fixation with multiple cannulated screws or a sliding hip screw (SHS).^{3–5} For most stable fracture patterns, multiple cannulated screws provide a relatively

Address for correspondence: Yuan Xue, Department of Orthopaedic Surgery, Tianjin Medical University General Hospital, 154 Anshan Road, Heping District, Tianjin, 300052, P. R. China. Email: xueyuanzy@163.com Yu Dai, Institute of Robotics and Automatic Information System, Nankai University, Room 116, Building of the College of Artificial Intelligence, No.38, Tong Yan Street, Jin Nan District, Tianjin, 300350, P. R. China. Email: daiyu@nankai.edu.cn Ping Lei, Department of Geriatrics, Tianjin Medical University General Hospital, 154 Anshan Road, Heping District, Tianjin, 300052, P. R. China. Email: leiping_1974@163.com

Sources of financial support: National Natural Science Foundation of China (Grant No: 62173190 and U1913207).

Received 5 May 2022; accepted 24 August 2022

minimally invasive technique, shorter operative time, and sufficient fixation capacity than SHS.^{6–10} If multiple cannulated screws and SHS are both appropriate for fracture fixation, screws should be used because they are less expensive. Therefore, multiple cannulated screws are crucial for a stable hip fracture.

Three cannulated screws are inserted in a parallel inverted triangle configuration (inferior, posteromedial, and anterosuperior) because they can provide high mechanical stability.^{11–15} Moreover, surgeons usually place the cannulated screws tightly on the posteromedial cortex and try to keep the screws inside the cortical bone, which provides better support and stabilization of the fracture area.^{16,17}

For fracture repositioning and fixation stability, surgeons place cannulated screws as close to the posteromedial cortex as possible; however, this operation is often performed using intraoperative fluoroscopy and is based on their own experience.¹⁸ An experienced surgeon can attach and even attempt to place the cannulated screws into the posteromedial cortex. However, some surgeons lack experience, and the accuracy varies owing to different personal experiences and inconsistencies in operations. If the posteromedial nail is placed completely into the cancellous bone, it will not provide sufficient stability and is predisposed to the collapse of the femoral neck and fixation failure.¹⁹ Moreover, a deviated nail can damage the surrounding vessels, such as the lateral epiphyseal artery, which can lead to femoral head necrosis.

In recent years, orthopaedic-assisted surgical robotics has been introduced to improve surgical safety.^{20–24} Currently, the application of orthopaedic-assisted surgical robotics is confined to passive system functions, such as navigation and pre-operative planning. However, an increasing number of surgeons are complaining about the robot's lack of semi-active and active functions, such as haptic feedback.^{25–28} Therefore, we designed a safe and easy-to-use robot-assisted method for automatic bone drilling and to distinguish critical bone drilling states with high accuracy in real-time for the bone hole-making process during hip fracture fixation.

The contributions of this investigation are as follows:

(i) investigate a safe and easy-to-use robot-assisted method for automatic bone drilling; (ii) use the drilling vibration signal to distinguish critical bone drilling states with high accuracy in real-time for the bone hole-making process during fixation of the femoral neck; (iii) apply the proposed method to avoid weak fixation and damage to the lateral epiphyseal artery during femoral neck fixation.

Materials and Methods

Drilling Mode Analysis During Fixation of Femoral Neck Fractures

To place the screw, the orthopaedist must first drill holes from the sidewall surface of the femur to the femoral head, as shown in Figure 1A. These holes passed through the entire femoral neck in an inverted triangle configuration. The screw is usually abutted against the cortical bone to

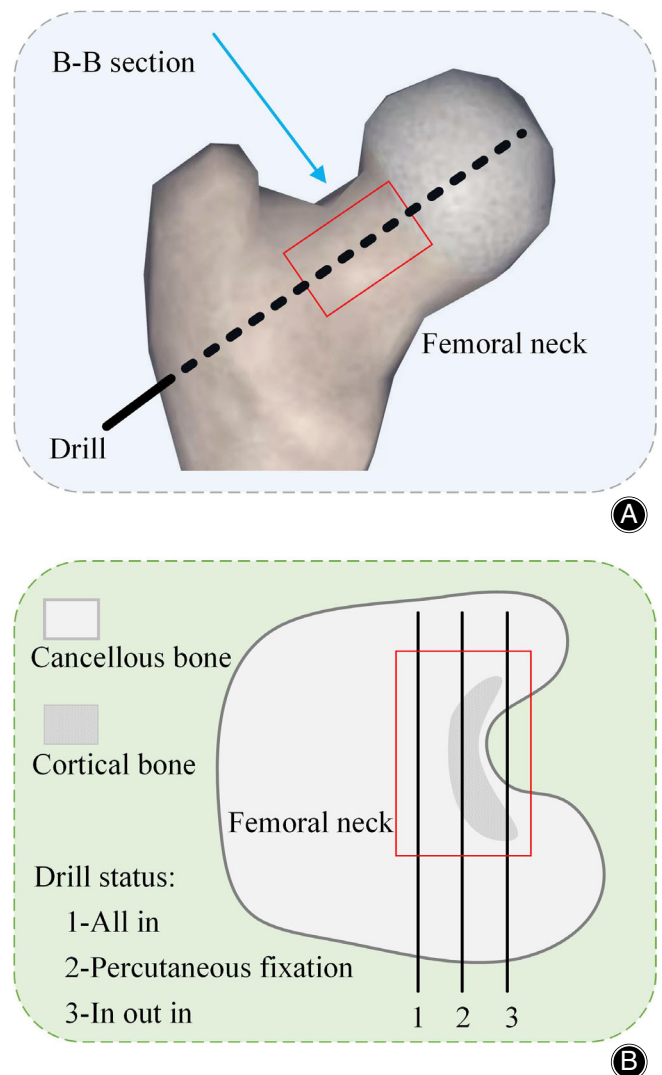


FIGURE 1 Three drilling modes during fixation of femoral neck fractures

improve the stability in the posterosuperior femoral neck. Figure 1B shows three possible drilling modes in the posterosuperior femoral neck: all in the cancellous bone (called “all-in,” AI), through the cortical bone (called “percutaneous fixation,” PF), and out the femoral neck (called “in-out-in,” IOI). The AI mode has a weak fixation construct. Therefore, surgeons should better distinguish between the AI and PF modes to avoid weak fixation. IOI mode may damage the lateral epiphyseal artery, which can cause femoral head necrosis. Therefore, the drilling operation must be stopped immediately when the drill end breaks through and out of the femoral neck to prevent harm to the artery.

Drilling Vibration Signal Acquisition

An experimental setup was designed to acquire the drilling vibration signals, as shown in Figure 2. The bone-drilling

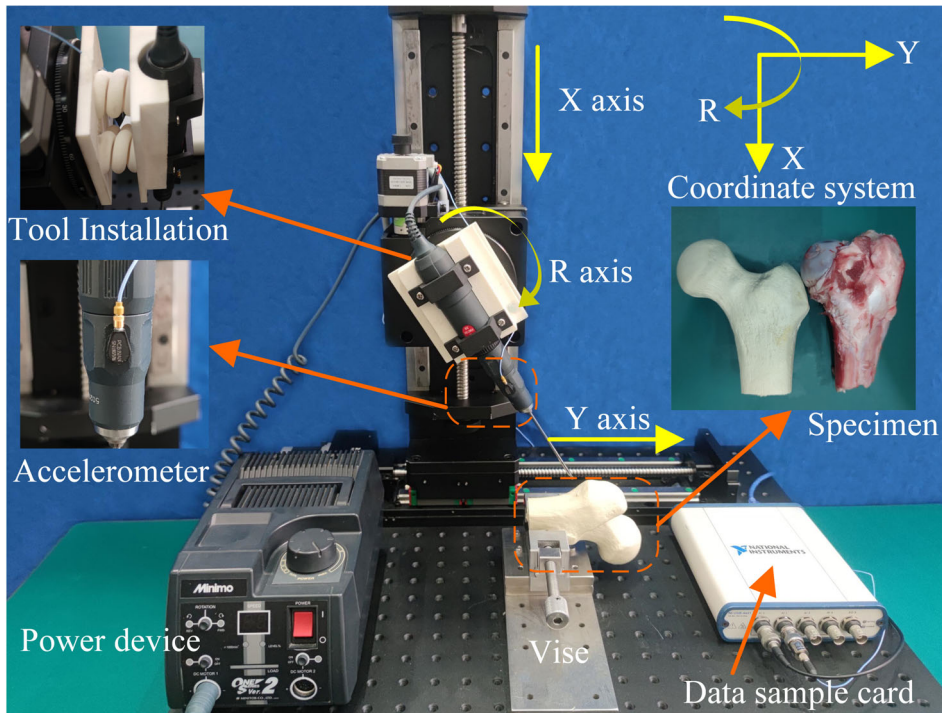


FIGURE 2 Experimental setup

robotic system consists of one rotation joint (TBR100, ZoliX, China) and two translation joints (PSA200, ZoliX, China). The rotation joint (R-axis) is used to adjust the drilling angle, and two translation joints (X-axis and Y-axis) can realize the linear motion of the drill along the adjusted angle. The drill is mounted at the end of the rotation joint by a specially designed installation unit to simulate the surgeon's hand and prevent potential resonance between the drill and robot arm. A high-frequency accelerometer (A1, PCB, USA) is glued to the surface of the drill handle. The power device (Minimo, Japan) can provide a max speed of 30,000 rounds per minute (RPM) to the drill. Four pig femurs were harvested from 6-month-old pigs (weight range, 24–30 kg; two females and two males) and drilled in this study, and each bone was fixed on a vise. The pig model was chosen because of its similarity to human femurs and its ease of acquisition. The bone-drilling robot was employed to drill each femur three times to contain AI, PF, and IOI drilling modes. The accelerometer captured the generated vibrations of the drill handle at a sampling frequency of 30 kHz. The captured vibrations were then transferred to a personal computer using an NI USB-4431 data-acquisition card.

Vibration Signal Processing

Figure 3 shows the raw drilling vibration signals captured at three different drill modes. Unlike in actual surgery, we can easily use dissections to observe drill states during *in vitro* drilling. Before the orange vertical line, vibrations were captured during the drilling of the femur. The vibrations after the orange vertical line were captured when

drilling the femoral neck and head. The captured vibrations are usually unstable during the initial drilling phase (between the blue and yellow lines). When the drilling vibration reached a stable level, the drill was observed in the cancellous bone of the femoral neck in the three different drilling modes. In the AI mode, the drill is further drilled into the cancellous bone of the femoral neck and head. In the IOI mode, the drill is first drilled out of the femoral neck and then into the cancellous bone of the femoral head. In the PF mode, the drill is further drilled into the cortical bone of the femoral neck and then into the cancellous bone of the femoral head. It can be intuitively seen that during the drilling out of the femoral neck, the absolute vibration amplitude of the drill handle will decrease slightly, and when the drill is in the cortical bone of the femoral neck, the absolute vibration amplitude of the drill handle will have a significant increase.

However, the absolute amplitude is not a stable value for distinguishing the drilling state because it is susceptible to interference from the drilling conditions, such as the drilling feed speed. The vibration signal is composed of a series of harmonic components. The frequency of these harmonics is an integer multiple of the drilling rotation frequency. Therefore, in this study, the harmonic distribution was used to identify the drilling characteristics. Fast Fourier Transformation (FFT) is an effective method for analyzing the harmonic distribution of a signal. Figures 4–6 show the FFT amplitude spectrum of the captured vibrations during three different drilling states: “in the cancellous bone,” “out the femoral neck,” and “in the cortical bone.”

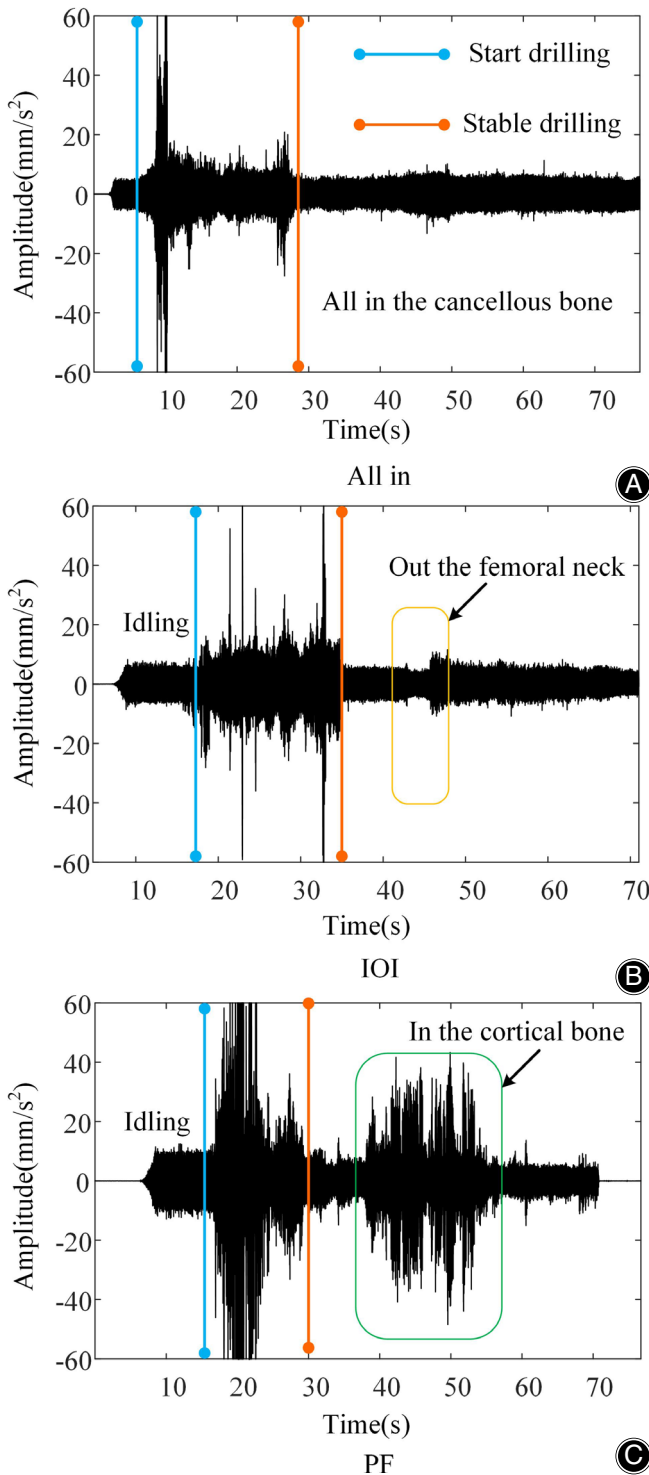


FIGURE 3 Raw drilling vibration signals captured at three drill modes

The sampling frequency F_s of the vibration signal used in this study is 30 kHz, and the duration T_s of each analyzed frame of vibration signal is 0.1 s, so the length of one frame of vibration signal N is 30000. The vibration signal is

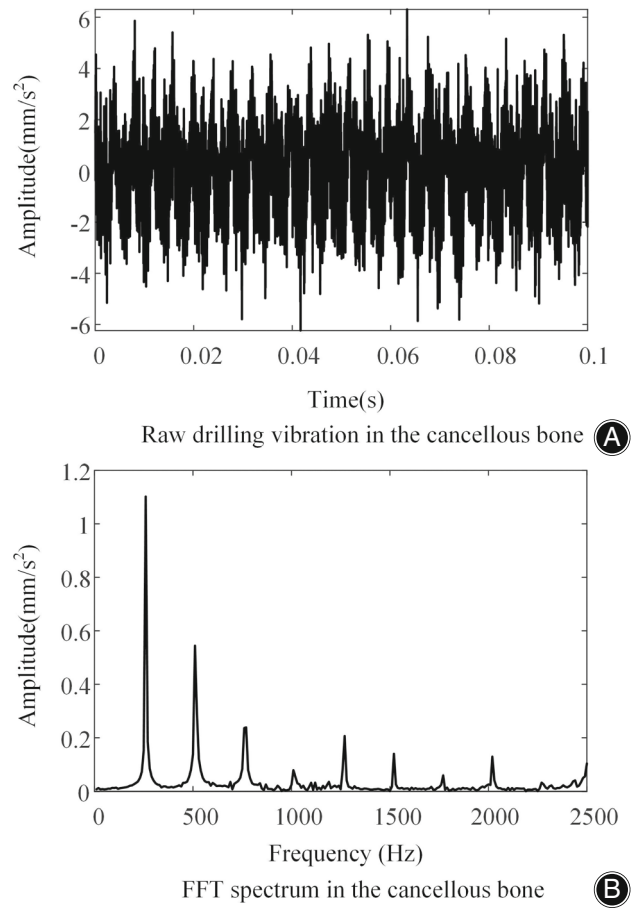


FIGURE 4 Drilling vibration of 0.1 s and its FFT in the cancellous bone

represented as $S_{1 \times N} = [S(1) S(2) \dots S(N)]$, and the signal after the FFT calculation is recorded as $F_{1 \times N} = [F(1) F(2) \dots F(N)]$. Considering that the rotational frequency of the drill may be attenuated by drilling the bone tissue, the robust i^{th} harmonic amplitude A_i can be calculated as follows:

$$r = F_c \times T_s = 500 \times 0.1 = 50 \quad (1)$$

$$A_i = \sum_{i=0.5 \times i \times r}^{1.5 \times i \times r} F(i) \quad (2)$$

where F_c is the rotational frequency of the drill (in this study, the rotational speed of the drill is 15000 RPM, i.e., the frequency is 250 Hz), and r is the center retrieval coefficient of the first harmonic.

As shown in Figures 4–6, when drilling in the cancellous bone of the femoral neck, the pivotal coefficients of the FFT are the first three harmonic amplitudes. When the femoral neck is drilled out, the pivotal coefficients of the FFT are the first-harmonic amplitudes. Moreover, when the drill is in the cortical bone of the femoral neck, the pivotal coefficients of the FFT are the first 10 harmonic amplitudes. Therefore,

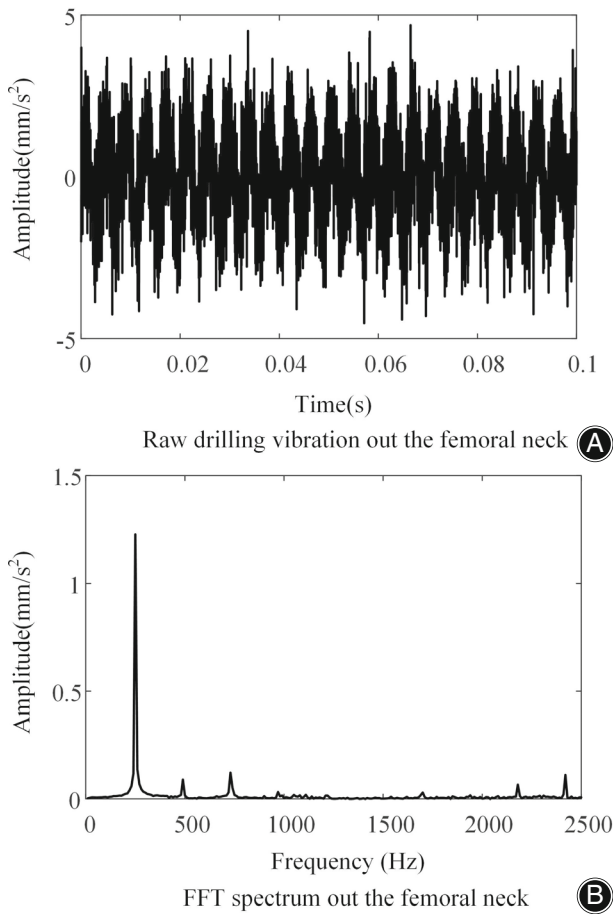


FIGURE 5 Drilling vibration of 0.1 s and its FFT out the femoral neck

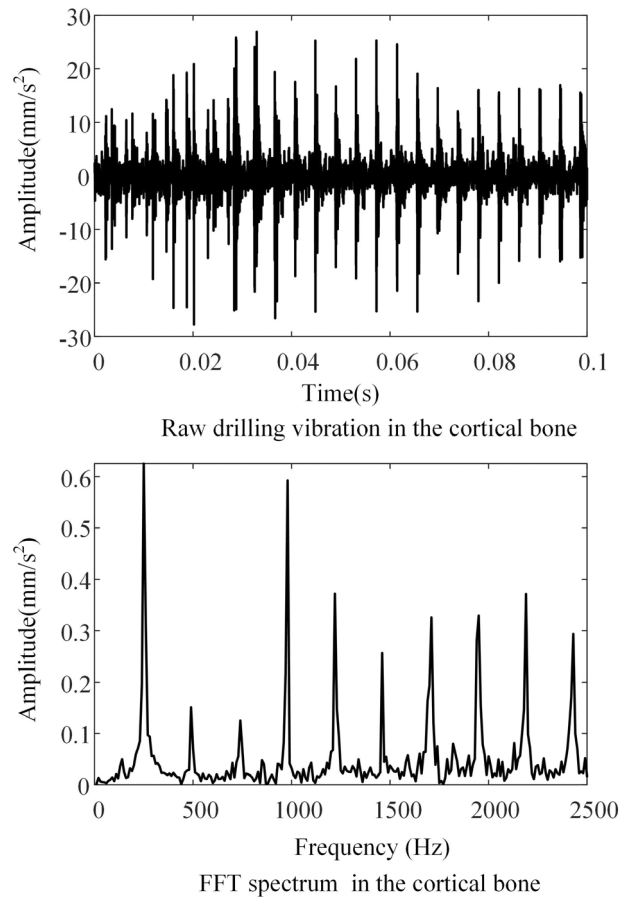


FIGURE 6 Drilling vibration of 0.1 s and its FFT in the cortical bone

the proportion A_{rel1} of the first harmonic in the first 10 harmonics is used to distinguish the drilling states and can be calculated as follows:

$$A_{rel1} = \frac{A_1}{\sum_{i=1}^{10} A_i}, \quad (3)$$

where A_i is the absolute value of i^{th} harmonic amplitude.

Drilling Status Recognition Method

A three-layered back propagation artificial neural network (BP-ANN) classifier is established to monitor the drilling status in real-time (0.01 s). The topology of the BP neural network is shown in Figure 7, where X_1, X_2, \dots, X_n are the input values of the BP-ANN, Y are the predicted drilling states, and w_{ij} and w_{jk} are the network weights. w_{ij} is the connection weight between the i^{th} neuron in the input layer and j^{th} neuron in the hidden layer, and w_{jk} is the connection weight between the j^{th} neuron in the hidden layer and k^{th} neuron in the output layer.

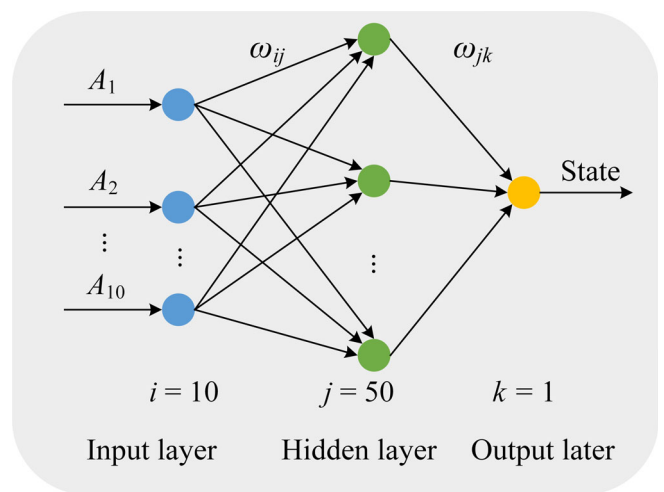


FIGURE 7 Three-layer back propagation artificial neural network

memory and prediction through training. Cross-entropy is used to train the network, and a confusion matrix is used to evaluate the performance of the network. To train the state

classifier, the data were further divided into many 0.01 s frames, and each frame of the data was marked with one drilling state.

Results

Analysis of Spectrum Difference Between Drilling States

The “lillietest” function of MATLAB is used to check whether the 50 A_{rel} data of each drilling state follow a normal distribution. Table 1 shows the normal distribution test results for five drilling states on four specimens, where l is the statistics, cv is the reference, and $p > 0.05$ is considered normally distributed. A_{rel} data for all specimens and different drilling states are normally distributed, indicating that the independent sample t-test can be applied to analyze the difference in A_{rel} for different drilling states.

Table 1 also shows the lower bound L and the upper bound U of the confidence intervals of each drilling state on the four specimens. Figures 8–11 show the raw data of A_{rel} , mean \pm SD of A_{rel} , and significant difference analysis results of the five drilling states on each specimen. The drilling states are compared in pairs, and states with no significant differences are highlighted with “NS.”

Every two adjacent states in the same specimen significantly differ in A_{rel} . Except for state 2, there is a slight standard deviation of A_{rel} for the other four states of all four specimens. Moreover, the mean values of A_{rel} from large to small are state 1, state 3, state 4, and state 5 for all four specimens. Although A_{rel} follows the above-mentioned qualitative law, it remains difficult to judge the drilling status by setting the threshold value due to the overlapping intervals between the A_{rel} values of different specimens. Moreover, state 2 is an unstable state that is prone to misjudgment. Therefore, A_{rel} can be an excellent reference to prove the difference in spectral distribution at the five typical drilling

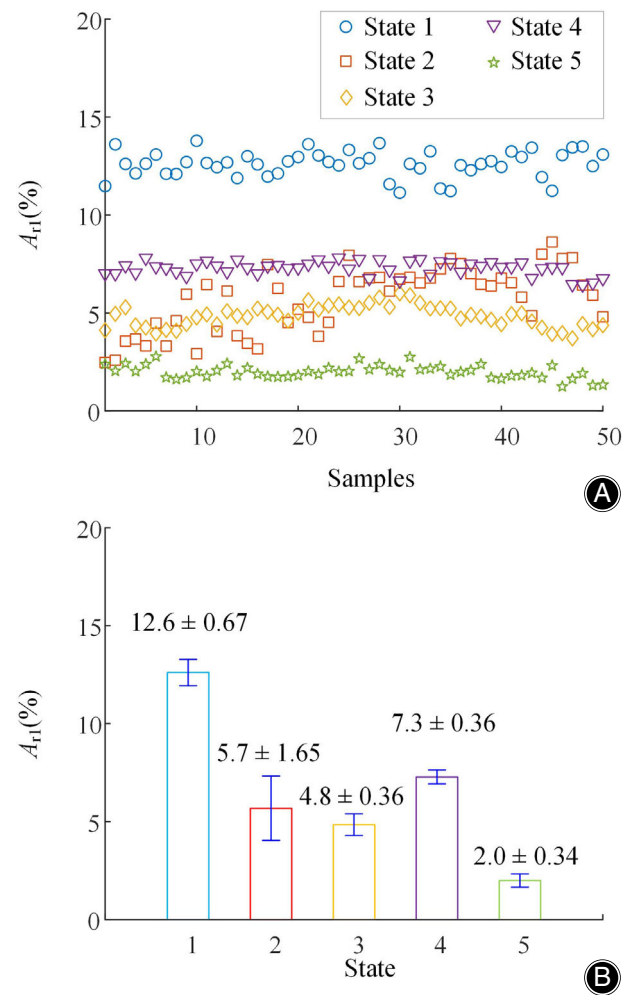


FIGURE 8 Raw data of A_r , mean \pm SD of A_r , and significant difference analysis results of five drilling states on specimen 1

TABLE 1 Normal distribution test result for five drilling states on four specimens

Specimen		State 1	State 2	State 3	State 4	State 5
1	l	0.1030	0.1444	0.0868	0.1269	0.0782
	cv	0.1451	0.1451	0.1451	0.1451	0.1451
	L	12.4173	5.2153	4.6852	7.1820	1.8977
	U	12.7979	6.1505	4.9997	7.3847	2.0898
	p	0.1986	0.0105	0.4326	0.0423	0.5000
2	l	0.0694	0.0917	0.1014	0.0734	0.0578
	cv	0.1451	0.1451	0.1451	0.1451	0.1451
	L	17.8812	2.6229	6.5552	15.0212	2.7915
	U	18.4305	2.9973	7.2660	15.4805	2.9692
	p	0.5000	0.3487	0.2184	0.5000	0.5000
3	l	0.1005	0.0914	0.0991	0.0944	0.0803
	cv	0.1451	0.1451	0.1451	0.1451	0.1451
	L	12.9538	13.9656	5.7677	8.2691	2.1016
	U	13.2266	16.6251	6.2319	8.5649	2.3994
	p	0.2294	0.3532	0.2475	0.3093	0.5000
4	l	0.0802	0.0839	0.0886	0.0842	0.1032
	cv	0.1451	0.1451	0.1451	0.1451	0.1451
	L	9.9347	24.4158	3.4174	7.2415	3.7853
	U	10.2981	25.3034	3.5962	7.5091	4.0568
	p	0.5000	0.5000	0.3991	0.4927	0.1965

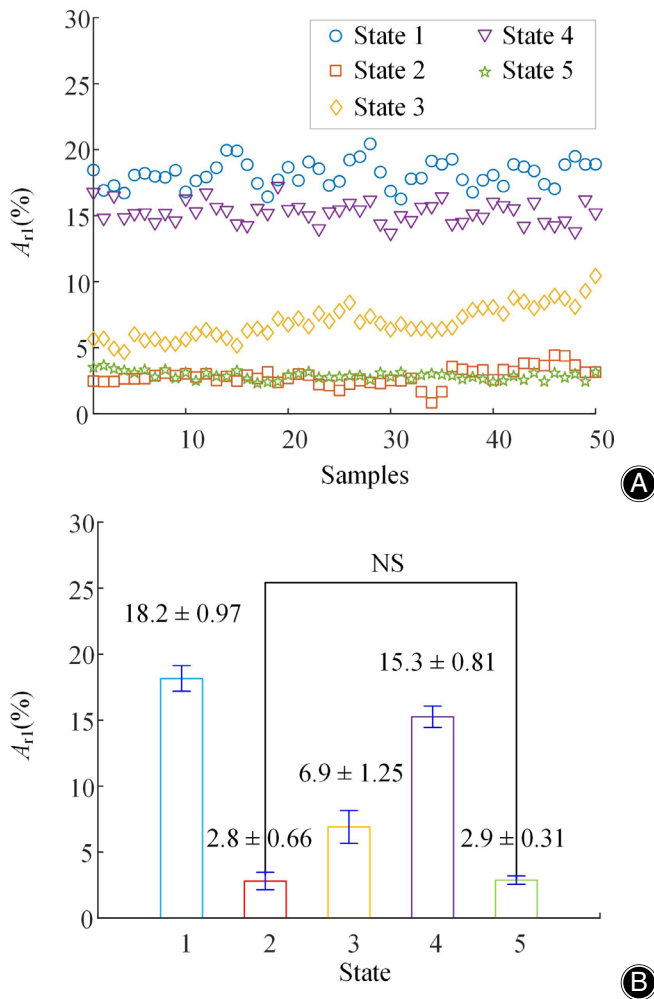


FIGURE 9 Raw data of A_r , mean \pm SD of A_r , and significant difference analysis results of five drilling states on specimen 2

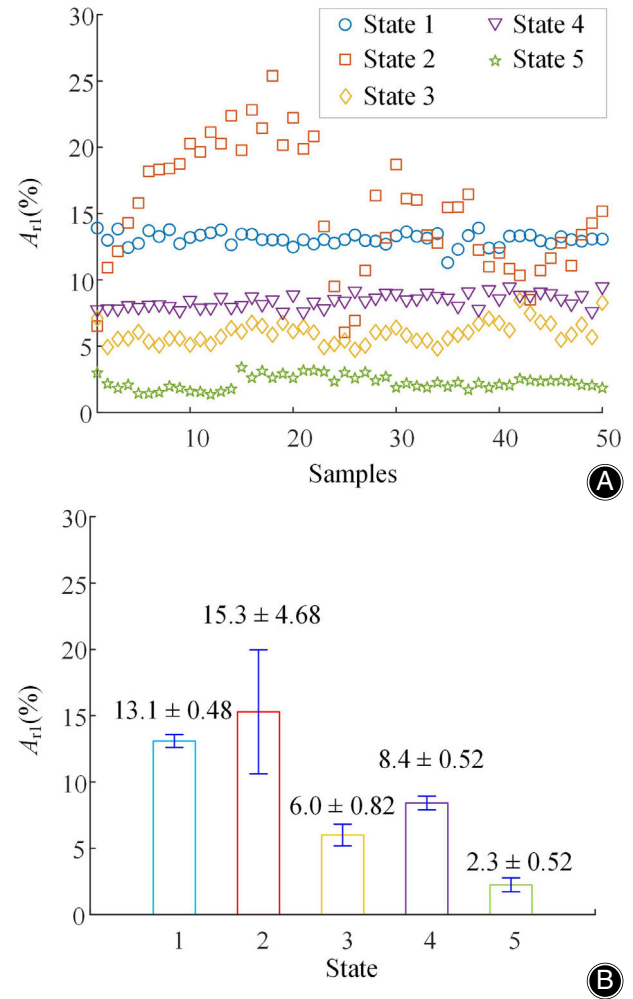


FIGURE 10 Raw data of A_r , mean \pm SD of A_r , and significant difference analysis results of five drilling states on specimen 3

states, although without high accuracy and robust index to recognize the drilling state directly.

Automatic Identification of Five Different Drilling States

The above results for A_r in different drilling states indicate that the drilling vibration signals have different spectral distributions in different states. These five states can be effectively identified using spectral information. Therefore, we trained a neural network classifier with the frequency spectrum as the input and drilled state as the output. The model was first trained using a dataset of four specimens. To avoid overfitting problems, data are randomly divided into three parts at ratios of 0.7, 0.15, and 0.15 for training, validation, and testing, respectively. We adjust the connection weights of the network according to errors in the training dataset, and the training progress stops when generalization stops improving on the validation dataset. Finally, the performance of the network will be tested using a test dataset.

Figures 12–15 show the recall and accuracy of the neural network classifier on the four specimens, where the bottom line is the recall rate, and the rightmost line is the accuracy rate. The training epochs of the neural network classifier for specimens 1–4 were 62, 78, 57, and 72. The recall rates of “in the cancellous bone” for specimens 1 to 4 were 96.3%, 83.7%, 88.0%, and 88.0%. The recall rates of “in out the femoral neck” from specimens 1 to 4 were 97.2%, 76.2%, 93.7%, and 94.4%. The recall rates of “in the cancellous bone” for specimens 1 to 4 were 97.8%, 92.3%, 100%, and 97.7%. The average recognition accuracies of the drilling state for specimens 1 to 4 were 86.8%, 84.7%, 95.2%, and 85.8%. Moreover, the critical drilling states can be distinguished with extremely high accuracy. The recognition accuracies of “in the cancellous bone” for specimens 1 to 4 were 83.2%, 84.8%, 92.9%, and 84.7%. The recognition accuracies of “in out the femoral neck” from specimens 1 to 4 were 98.2%, 88.4%, 95.8%, and 88.7%. The recognition accuracies

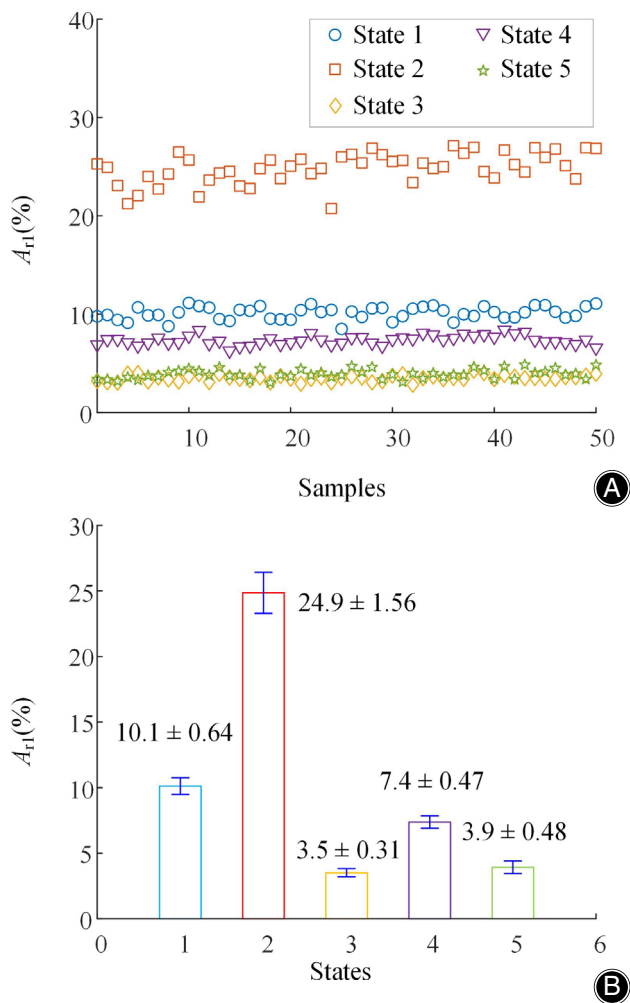


FIGURE 11 Raw data of A_r , mean \pm SD of A_r , and significant difference analysis results of five drilling states on specimen 4

of “in the cortical bone” for specimens 1 to 4 were 94.6%, 80.8%, 95.5%, and 88.9%.

Discussion

Because traditional manual drilling during hip fracture fixation can easily lead to unstable fixation and vascular damage. A safe and easy-to-use robot-assisted method to automatically drill bone and distinguish critical bone drilling states with high accuracy in real-time for the bone hole-making process during hip fracture fixation is urgently needed. In this study, a safe and easy-to-use robot-assisted method is proposed for automatic bone drilling and to distinguish critical bone drilling states with high accuracy in real-time for the bone hole-making process during femoral neck fixation. Four fresh pig femurs were drilled at the posterosuperior femoral neck in three modes, and five bone-drilling states were defined. We proved the difference in the harmonic distribution at different drilling states using an independent sample t-test. To distinguish the critical bone drilling states

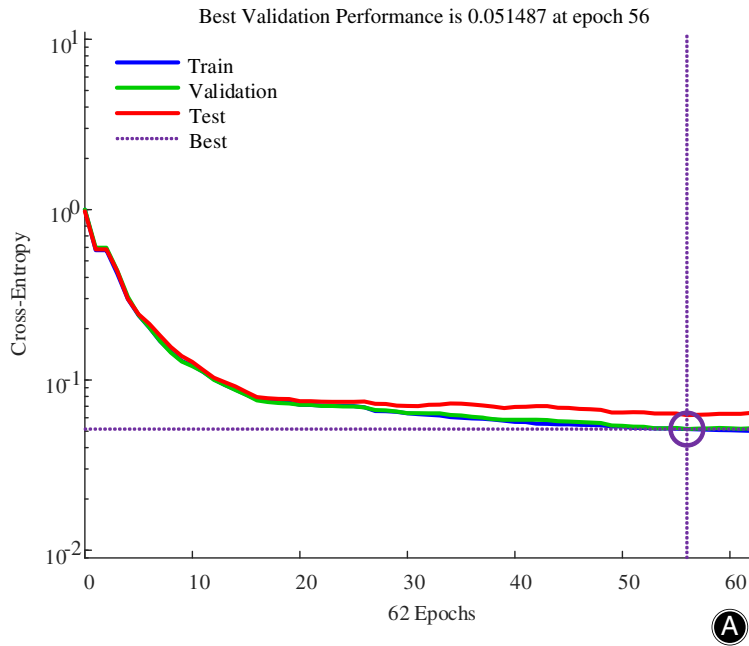
with high accuracy in real-time, a neural network classifier was trained with the frequency spectrum as the input and the drilled state as the output. The average recognition accuracies of the drilling state for the four specimens were all higher than 84%. Critical drilling states can be distinguished with extremely high accuracy. Our method can potentially prevent weak fixation and damage to the lateral epiphyseal artery. From the working principle, the identification of bone drilling state has a strong correlation with parameters such as bone type and whether it is drilled. Therefore, the proposed robotic bone hole fabrication strategy can actually be applied to improve drilling safety in other orthopaedic surgeries, such as spine and trauma surgeries, and is scalable. In our future work, we will expand our specimen size, such as including cases of osteosclerosis and osteoporosis, to further demonstrate the validity and accuracy of our study.

Challenges of Drilling Task in Traditional Hip Fractures Fixation

In recent years, with the increasing number of patients undergoing hip fracture surgery, internal fixation of hip fractures has become the focus of discussion. Impacted and non-displaced femoral neck fractures and stable intertrochanteric fractures usually involve *in situ* fixation with either multiple cannulated screws or SHS.^{29,30} Compared with SHS, multiple cannulated screw fixation has the advantages of low revision surgery rate, high survival rate, short operation time, less bleeding, low risk of osteonecrosis, and cost saving.⁵ Therefore, multiple cannulated screw fixation remains an important and safe surgical procedure to stabilize hip fractures. However, multiple cannulated screw fixations are affected by the surgeon’s experience. The unstable bare-handed operation, visual deviation, and degree of fracture reduction make it difficult to ensure the success of a one-time puncture when the guide pin is punctured. The number of drills and adjusting the guide pin puncture path attempt should be kept to a minimum during the surgery, as they can weaken the cortical and cancellous bone, re-injure muscles, soft tissues, and bones, increase the degree of surgical trauma, and increase the amount of bleeding in patients. At the same time, prolonging the operation time, extensive use of fluoroscopy, and increasing the exposure time may endanger the patient and operating room staff. Reference indicates that the femoral head’s avascular necrosis was observed in 12 cases (23%) and nonunion was observed in five cases (9%) during their follow-up periods.³¹

Advantages and Disadvantages of Current Robot-Assisted Operations in Hip Fracture Fixation

With the development and updating of medical imaging and computer technologies, computer-assisted orthopaedic surgery has been widely used in joint surgery, spine surgery, and traumatic orthopaedics.²⁰ The stereotactic technique based on X-ray or three-dimensional (3D) CT images can assist surgeons in planning surgeries more precisely, improving surgical efficiency and accuracy, reducing radiation



1	235 10.2%	0 0.0%	3 0.1%	0 0.0%	0 0.0%	98.7% 1.3%
2	0 0.0%	52 2.3%	18 0.8%	2 0.1%	0 0.0%	72.2% 27.8%
3	8 0.3%	208 9.1%	1139 49.7%	3 0.1%	8 0.3%	83.4% 16.6%
4	1 0.0%	2 0.1%	1 0.0%	272 11.9%	0 0.0%	98.6% 1.4%
5	0 0.0%	0 0.0%	15 0.7%	0 0.0%	327 14.3%	95.6% 4.4%
	96.3% 3.7%	19.8% 80.2%	96.9% 3.1%	98.2% 1.8%	97.6% 2.4%	88.3% 11.7%
	↖	↖	↖	↖	↖	

Target state

Training Confusion Matrix

1	56 11.4%	0 0.0%	0 0.0%	1 0.2%	0 0.0%	98.2% 1.8%
2	0 0.0%	6 1.2%	9 1.8%	0 0.0%	0 0.0%	40.0% 60.0%
3	3 0.6%	46 9.4%	235 47.9%	0 0.0%	0 0.0%	82.7% 17.3%
4	0 0.0%	1 0.2%	1 0.2%	56 11.4%	0 0.0%	96.6% 3.4%
5	0 0.0%	0 0.0%	3 0.6%	1 0.2%	73 14.9%	94.8% 5.2%
	94.9% 5.1%	11.3% 88.7%	94.8% 5.2%	96.6% 3.4%	100% 0.0%	86.8% 13.2%
	↖	↖	↖	↖	↖	

Target state

Validation Confusion Matrix

1	60 12.2%	0 0.0%	2 0.4%	1 0.2%	0 0.0%	95.2% 4.8%
2	0 0.0%	12 2.4%	6 1.2%	0 0.0%	0 0.0%	66.7% 33.3%
3	1 0.2%	48 9.8%	242 49.3%	0 0.0%	2 0.4%	82.6% 17.4%
4	0 0.0%	1 0.2%	0 0.0%	57 11.6%	0 0.0%	98.3% 1.7%
5	0 0.0%	0 0.0%	4 0.8%	3 0.6%	52 10.6%	88.1% 11.9%
	98.4% 1.6%	19.7% 80.3%	95.3% 4.7%	93.4% 6.6%	96.3% 3.7%	86.2% 13.8%
	↖	↖	↖	↖	↖	

Target state

Test Confusion Matrix

1	351 10.7%	0 0.0%	5 0.2%	2 0.1%	0 0.0%	98.0% 2.0%
2	0 0.0%	70 2.1%	33 1.0%	2 0.1%	0 0.0%	66.7% 33.3%
3	12 0.4%	302 9.2%	1616 49.3%	3 0.1%	10 0.3%	83.2% 16.8%
4	1 0.0%	4 0.1%	2 0.1%	385 11.8%	0 0.0%	98.2% 1.8%
5	0 0.0%	0 0.0%	22 0.7%	4 0.1%	452 13.8%	94.6% 5.4%
	96.4% 3.6%	18.6% 81.4%	96.3% 3.7%	97.2% 2.8%	97.8% 2.2%	87.7% 12.3%
	↖	↖	↖	↖	↖	

Target state

All Confusion Matrix

FIGURE 12 Training results on specimen 1. (A) Performance curve; (B) Recall and accuracy of the neural network classifier

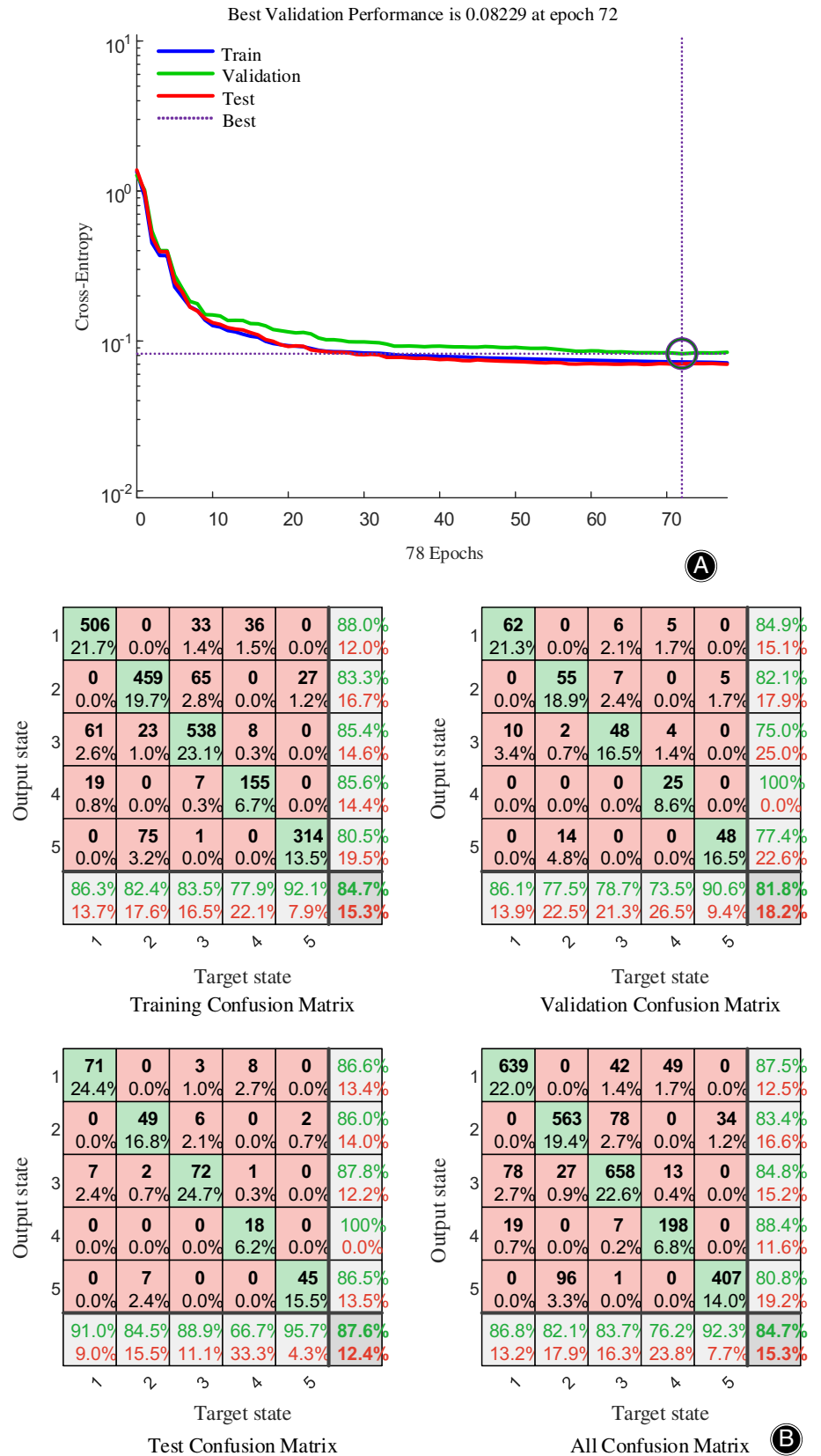
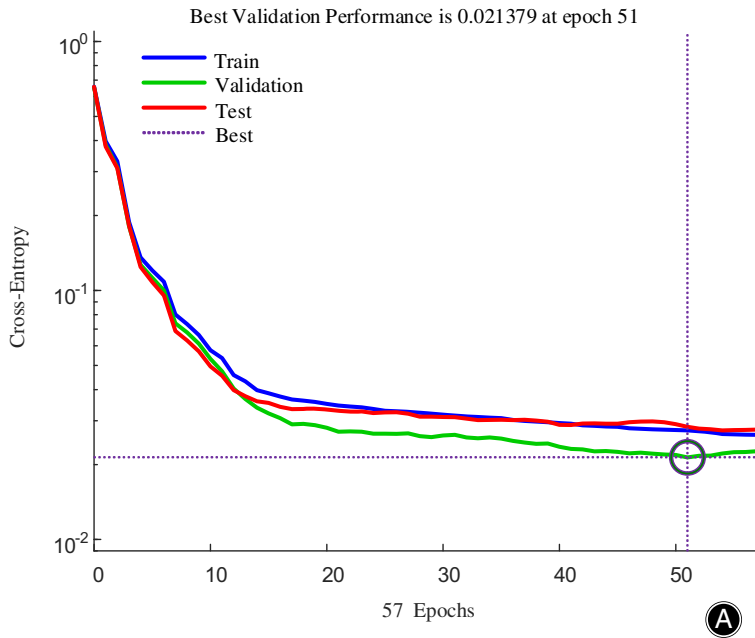


FIGURE 13 Training results on specimen 2.
(A) Performance curve; (B) Recall and accuracy of the neural network classifier



Output state	1	2	3	4	5	
	647 33.1%	1 0.1%	22 1.1%	0 0.0%	0 0.0%	96.6%
	6 0.3%	335 17.2%	15 0.8%	0 0.0%	0 0.0%	94.1%
	10 0.5%	7 0.4%	391 20.0%	15 0.8%	0 0.0%	92.4%
	2 0.1%	0 0.0%	7 0.4%	209 10.7%	0 0.0%	95.9%
	0 0.0%	0 0.0%	13 0.7%	0 0.0%	272 13.9%	95.4%
	97.3%	97.7%	87.3%	93.3%	100%	95.0%
	2.7%	2.3%	12.7%	6.7%	0.0%	5.0%
	1	2	3	4	5	
	Target state					

Training Confusion Matrix

Output state	1	2	3	4	5	
	140 33.5%	1 0.2%	4 1.0%	0 0.0%	0 0.0%	96.6%
	0 0.0%	66 15.8%	1 0.2%	0 0.0%	0 0.0%	98.5%
	2 0.5%	1 0.2%	94 22.5%	3 0.7%	0 0.0%	94.0%
	0 0.0%	0 0.0%	1 0.2%	41 9.8%	0 0.0%	97.6%
	0 0.0%	0 0.0%	4 1.0%	0 0.0%	60 14.4%	93.8%
	98.6%	97.1%	90.4%	93.2%	100%	95.9%
	1.4%	2.9%	9.6%	6.8%	0.0%	4.1%
	1	2	3	4	5	
	Target state					

Validation Confusion Matrix

Output state	1	2	3	4	5	
	151 36.1%	1 0.2%	5 1.2%	0 0.0%	0 0.0%	96.2%
	1 0.2%	69 16.5%	2 0.5%	0 0.0%	0 0.0%	95.8%
	3 0.7%	1 0.2%	87 20.8%	2 0.5%	0 0.0%	93.5%
	0 0.0%	0 0.0%	3 0.7%	45 10.8%	0 0.0%	93.8%
	0 0.0%	0 0.0%	1 0.2%	0 0.0%	47 11.2%	97.9%
	97.4%	97.2%	88.8%	95.7%	100%	95.5%
	2.6%	2.8%	11.2%	4.3%	0.0%	4.5%
	1	2	3	4	5	
	Target state					

Test Confusion Matrix

Output state	1	2	3	4	5	
	938 33.6%	3 0.1%	31 1.1%	0 0.0%	0 0.0%	96.5%
	7 0.3%	470 16.9%	18 0.6%	0 0.0%	0 0.0%	94.9%
	15 0.5%	9 0.3%	572 20.5%	20 0.7%	0 0.0%	92.9%
	2 0.1%	0 0.0%	11 0.4%	295 10.6%	0 0.0%	95.8%
	0 0.0%	0 0.0%	18 0.6%	0 0.0%	379 13.6%	95.5%
	97.5%	97.5%	88.0%	93.7%	100%	95.2%
	2.5%	2.5%	12.0%	6.3%	0.0%	4.8%
	1	2	3	4	5	
	Target state					

All Confusion Matrix

FIGURE 14 Training results on specimen 3. (A) Performance curve; (B) Recall and accuracy of the neural network classifier

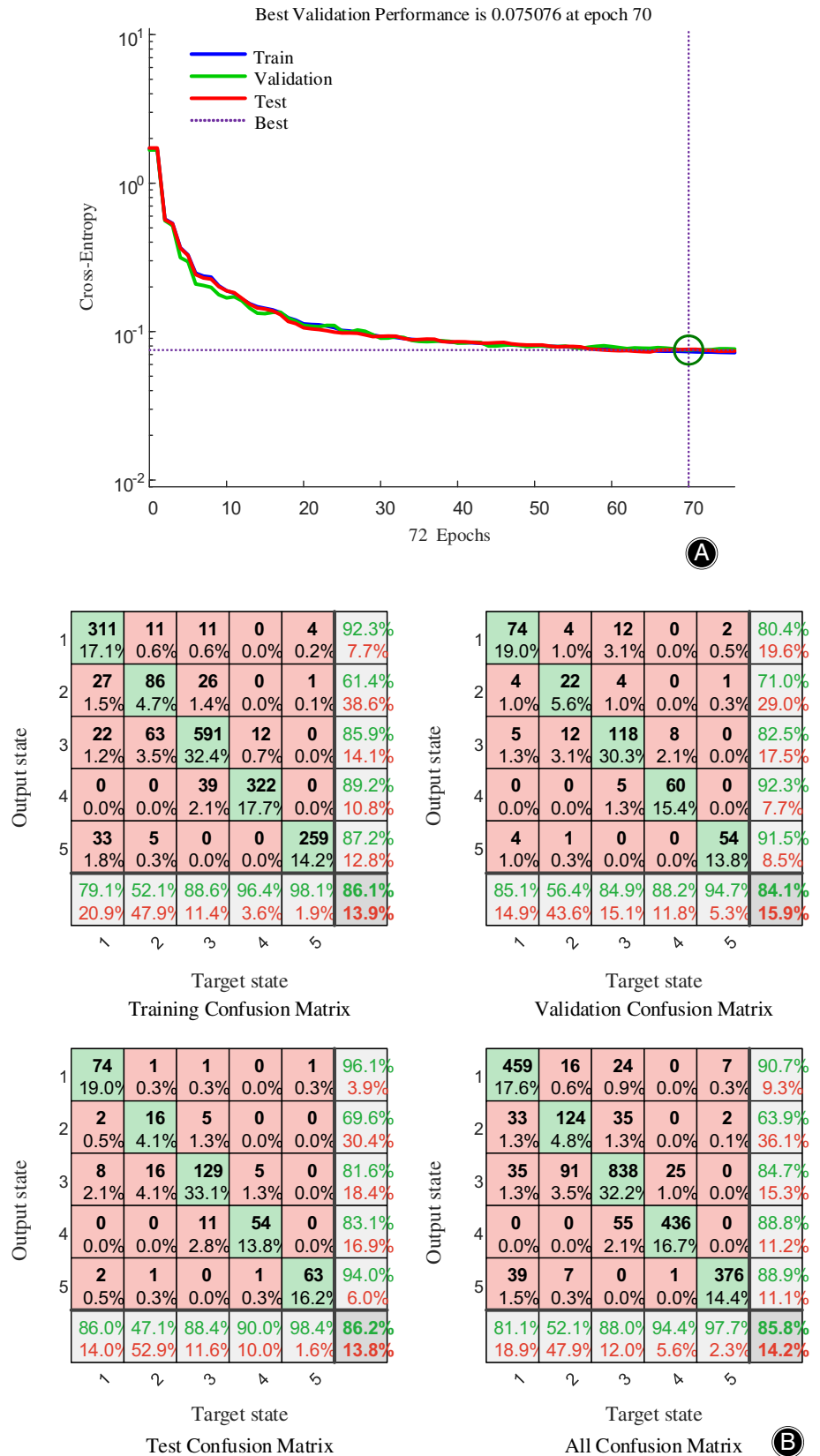


FIGURE 15 Training results on specimen 4.
(A) Performance curve; (B) Recall and accuracy of the neural network classifier

exposure, and reducing patient injury.³² However, computer-assisted orthopaedic surgery is not perfect.²⁴ Current computer-assisted orthopaedic surgery has limitations in terms of positioning and navigation. Navigation orthopaedist-assisted robots have significant advantages over traditional freehand operations. However, key intraoperative steps need to be performed by experienced surgeons with their bare hands, which also greatly reduces the safety, reliability, and ease of computer-assisted orthopaedic surgery. With advances in technology and surgical innovation, an increasing number of surgeons are complaining of the lack of tactile feedback from computer-assisted and robotic techniques. As a result, considerable research is currently underway to overcome this barrier.

Comparisons With Other Bone Drilling State Identification Methods

The main results of this study can be summarized as follows. In each specimen, the harmonic distributions of the drilling vibration at each of the two adjacent drilling modes were statistically different ($p < 0.05$). The average recognition accuracies of the drilling state for the four specimens exceed 84%. Moreover, the critical drilling states can be distinguished with extremely high accuracy. The recognition accuracies of “in the cancellous bone” for specimens 1 to 4 were 83.2%, 84.8%, 92.9%, and 84.7%. The recognition accuracies of “in out the femoral neck” from specimens 1 to 4 were 98.2%, 88.4%, 95.8%, and 88.8%. The recognition accuracies of “in the cortical bone” for specimens 1 to 4 were 94.6%, 80.8%, 95.5%, and 85.8%. The proposed robot-assisted method can potentially prevent weak fixation and damage to the lateral epiphyseal artery.

The bone-drilling process generates force, sound, and vibration signals that are composed of a series of harmonic signals. Dai *et al.* sampled the drill vibration signal with an accelerometer, and considering that the drilling sound signal and vibration signal are homologous, they combined these two signals for bone drilling state monitoring and successfully identified four different bone drilling states, as well as the entanglement state when the drill is wrapped by the muscle.³³ In 2021, they use of vibration signals to simulate human haptic feedback was proposed to perceive and control orthopaedic assisted surgery robots.³⁴ Hu *et al.* identified five primary drilling states by processing force signals in the drilling feed direction, including initial state, outer cortical state, cancellous state, transitional state, and inner cortical state.³⁵ In 2020, Torun *et al.* proposed a breakthrough detection method based on the closed-loop control characteristics of the bone drilling process.³⁶ Our previous study found that there is an approximately linear relationship between harmonic amplitude and bone drilling depth for a specific range of cutting depths, and the bone drilling depth can be estimated using the amplitude of a specific harmonic over a certain range of cutting depths.^{37–40} This study extracts and analyzes the vibration signal features during hip fracture nailing based on the FFT transformation and enables the

orthopaedist-assisted surgical robot to accurately identify five states through the deep learning method of the BP-ANN classifier. Especially during posteromedial cannulated screw placement, it helps surgeons identify “all-in” (AI), “in-out-in” (IOI), and “percutaneous fixation” (PF) in real-time, avoiding injury to the surrounding blood vessels and nerves, and reducing the burden of the surgeon and the difficulty of surgery.

Strengths and Limitations

The orthopaedist-assisted surgical robot with learning *via* a BP-ANN classifier combined with preoperative navigation planning can sense and control the placement of multiple cannulated screws, which provides a new research direction for the future development of computer-assisted orthopedic robots and has the potential to further simplify surgical procedures. It can avoid repeated drilling and adjusting the guide pin puncture path and may assist the surgeon in better placement of multiple cannulated screws, especially posteromedial screws, making the operation more fluent. The posterior medial and lateral cortices under the vastus ridge play an important stabilizing role in hip fracture reduction and fixation. The orthopaedist-assisted surgery robot with deep learning can help surgeons more accurately insert posteromedial screws into the PF position, which can better stabilize the fracture, reduce the amount of bleeding, and make the surgery safer, conducive to fracture healing, and early rehabilitation exercises.

This study has some limitations. First, the study included *ex vivo* specimens; therefore, the patient’s regular movements (e.g., respiratory movements) during the surgery may have an impact on the accuracy of the experimental results. Next, we will conduct experiments on live animals. Second, the femoral neck of healthy pigs was selected for the experiment; therefore, the results of this experiment are only significant for hip fractures in non-pathological states. The next step is to expand our specimen size. Femoral necks in pathological states such as osteosclerosis and osteoporosis were selected for experiments to further demonstrate the validity and accuracy of our study. A more sophisticated classification method based on the vibration signal of the drill handle is expected to be designed in the future to identify bone types and to distinguish soft tissues, such as muscles, blood vessels, and ligaments. To improve identification accuracy, more *in vivo* bone drilling experiments must be performed to obtain sufficient data for network training.

Conclusion

This study investigated a safe and easy-to-use robot-assisted method to automatically drill bone and distinguish critical bone drilling states with high accuracy in real-time for the bone hole-making process during hip fracture fixation. The recognition accuracies of “in the cancellous bone” for specimens 1 to 4 were 83.2%, 84.8%, 92.9%, and 84.7%. The recognition accuracies of “in out the femoral

neck” from specimens 1 to 4 were 98.2%, 88.4%, 95.8%, and 88.8%. The recognition accuracies of “in the cortical bone” for specimens 1 to 4 were 94.6%, 80.8%, 95.5%, and 85.8%. The average recognition accuracies of the drilling state for the four specimens exceed 84%. The proposed robot-assisted method can potentially prevent weak fixation and damage to the lateral epiphyseal artery. In our future work, we will expand our specimen size, such as including cases of osteosclerosis and osteoporosis, to further demonstrate the validity and accuracy of our study.

Data Availability

Data are available on request from the corresponding author.

Author Contributions

Conceptualization: Yuan Xue, Yu Dai, Ping Lei, and Jianxun Zhang. Data curation: Guangming Xia and He Bai. Formal analysis: Guangming Xia and Wei Liu. Writing—original draft: Guangming Xia and Jianxun Zhang. Writing—review and editing: Guangming Xia, He Bai, Wei Liu, Yuan Xue, Ping Lei, and Yu Dai.

Conflicts of Interest

The authors declare that there are no conflicts of interest regarding the publication of this paper.

Funding Information

National Natural Science Foundation of China (62173190, U1913207).

References

- Socci AR, Casemyr NE, Leslie MP, Baumgaertner MR. Implant options for the treatment of intertrochanteric fractures of the hip: rationale, evidence, and recommendations. *Bone Joint J.* 2017;99:128–33.
- Adam M, Alkaramany E, Alhamoud A, Derbas J, Murshid A, Alhaneedi GA. Appropriateness of the post-operative rehabilitation of low energy hip fractures in elderly in comparison with the AAOS appropriate use criteria at a level one trauma center. *Eur J Orthop Surg Traumatol.* 2022;32:219–27.
- Zhao Y, Yin K, Zhao H, Peng Z. Multiple screws versus sliding hip screws in femoral neck fractures: a protocol of cohort study. *Medicine.* 2020;99:e20970.
- Xia Y, Zhang W, Zhang Z, Wang J, Yan L. Treatment of femoral neck fractures: sliding hip screw or cannulated screws? A Meta-Analysis. *J Orthop Surg Res.* 2021;16:54.
- Florschütz AV, Langford JR, Haidukewych GJ, Koval KJ. Femoral neck fractures: current management. *J Orthop Trauma.* 2015;29:121–9.
- Kain MS, Marcantonio AJ, Iorio R. Revision surgery occurs frequently after percutaneous fixation of stable femoral neck fractures in elderly patients. *Clin Orthop Relat Res.* 2014;472:4010–4.
- Gjertsen JE, Fevang JM, Matre K, Vinje T, Engesaeter LB. Clinical outcome after undisplaced femoral neck fractures. *Acta Orthop.* 2011;82:268–74.
- Chen YF, Ren D, Yao SQ, et al. Accurate placement of cannulated screws in femoral neck fractures: screw and guide wire combined technique. *Orthop Surg.* 2021;13:2472–6.
- Hsu MR, Shu HT, Luksameearunothai K, et al. Is there an increased risk for subtrochanteric stress fracture with the femoral neck system versus multiple cannulated screws fixation? *J Orthop.* 2022;30:127–33.
- Duan SJ, Liu HS, Wu WC, Yang K, Zhang Z, Liu SD. Robot-assisted percutaneous cannulated screw fixation of femoral neck fractures: preliminary clinical results. *Orthop Surg.* 2019;11:34–41.
- Zhang RY, Li JT, Zhao JX, et al. Comparison of oblique triangular configuration and inverted equilateral triangular configuration of three cannulated screws in treating unstable femoral neck fracture: a finite element analysis. *Injury.* 2022;53:353–61.
- Zdero R, Keast-Butler O, Schemitsch EH. A biomechanical comparison of two triple-screw methods for femoral neck fracture fixation in a synthetic bone model. *J Trauma.* 2010;69:1537–44.
- Zhang RY, Li JT, Zhao JX, et al. The oblique triangle configuration of three parallel screws for femoral neck fracture fixation using computer-aided design modules. *Sci Rep.* 2022;12:325.
- Papanastassiou ID, Mavrogenis AF, Kokkalis ZT, Nikolopoulos K, Skourtas K, Papanastassiou PJ. Fixation of femoral neck fractures using divergent versus parallel cannulated screws. *J Long Term Eff Med Implants.* 2011;21:63–9.
- Zhu J, Deng X, Hu H, Cheng X, Tan Z, Zhang Y. Comparison of the effect of rhombic and inverted triangle configurations of cannulated screws on internal fixation of nondisplaced femoral neck fractures in elderly patients. *Orthop Surg.* 2022;14:720–9.
- Griffin JB. The calcar femorale redefined. *Clin Orthop Relat Res.* 1982;164:211–4.
- Kauffman JI, Simon JA, Kummer FJ, Pearlman CJ, Zuckerman JD, Koval KJ. Internal fixation of femoral neck fractures with posterior comminution: a biomechanical study. *J Orthop Trauma.* 1999;13:155–9.
- Liu J, Zhang B, Yin B, Chen H, Sun H, Zhang W. Biomechanical evaluation of the modified cannulated screws fixation of unstable femoral neck fracture with comminuted posteromedial cortex. *Biomed Res Int.* 2019;2019:2584151.
- Huang ZY, Su YH, Huang ZP, et al. Medial buttress plate and allograft bone-assisted cannulated screw fixation for unstable femoral neck fracture with posteromedial comminution: a retrospective controlled study. *Orthop Surg.* 2022;14:911–8.
- Karthik K, Colegate-Stone T, Dasgupta P, Tavakkolizadeh A, Sinha J. Robotic surgery in trauma and orthopaedics: a systematic review. *Bone Joint J.* 2015;97:292–9.
- Zheng G, Nolte LP. Computer-assisted orthopedic surgery: current state and future perspective. *Front Surg.* 2015;23(2):66.
- Wang XD, Lan H, Li KN. Treatment of femoral neck fractures with cannulated screw invasive internal fixation assisted by orthopaedic surgery robot positioning system. *Orthop Surg.* 2019;11:864–72.
- Wan L, Zhang X, Wu D, et al. Application of robot positioning for cannulated screw internal fixation in the treatment of femoral neck fracture: retrospective study. *JMIR Med Inform.* 2021;9:e24164.
- Hernandez D, Garimella R, Eltorai AEM, Daniels AH. Computer-assisted orthopaedic surgery. *Orthop Surg.* 2017;9:152–8.
- Karponis D, Koya Y, Miyazaki R, Kanno T, Kawashima K. Evaluation of a pneumatic surgical robot with dynamic force feedback. *J Robot Surg.* 2019;13:413–21.
- Luo J, Yan YJ, Wang XD, Long XD, Lan H, Li KN. Accuracy and safety of robot-assisted drilling decompression for osteonecrosis of the femoral head. *Orthop Surg.* 2020;12:784–91.
- Bai H, Wang R, Wang Q, et al. Motor bur milling state identification via fast fourier transform analyzing sound signal in cervical spine posterior decompression surgery. *Orthop Surg.* 2021;13:2382–95.
- Shao F, Tang M, Bai H, Xue Y, Dai Y, Zhang J. Drilling condition identification based on sound pressure signal in anterior cervical discectomy surgery. *Med Sci Monit.* 2019;25:6574–80.
- Zhu ZD, Xiao CW, Tan B, et al. Tirobot-assisted percutaneous cannulated screw fixation in the treatment of femoral neck fractures: a minimum 2-year follow-up of 50 patients. *Orthop Surg.* 2021;13:244–52.
- Ma JX, Kuang MJ, Xing F, et al. Sliding hip screw versus cannulated cancellous screws for fixation of femoral neck fracture in adults: a systematic review. *Int J Surg.* 2018;52:89–97.
- Kim JY, Kong GM, Park DH, Kim DY. Multiple cannulated screw fixation of young femoral neck fractures. *Pak J Med Sci.* 2015;31(6):1517–20.
- Liu P, Lu FF, Liu GJ, et al. Robotic-assisted unicompartmental knee arthroplasty: a review. *Arthroplasty.* 2021;3:15.
- Dai Y, Xue Y, Zhang JX. Milling state identification based on vibration sense of a robotic surgical system. *IEEE Trans Ind Electron.* 2016;63:6184–93.
- Dai Y, Xue Y, Zhang J. Human-inspired haptic perception and control in robot-assisted milling surgery. *IEEE Trans Haptics.* 2021;14:359–70.
- Hu Y, Jin HY, Zhang LW, et al. State recognition of pedicle drilling with force sensing in a robotic spinal surgical system. *IEEE ASME Trans Mechatron.* 2014;19:357–65.
- Torun Y, Öztürk A. A new breakthrough detection method for bone drilling in robotic orthopedic surgery with closed-loop control approach. *Ann Biomed Eng.* 2020;48:1218–29.
- Xia GM, Dai Y, Zhang JX, et al. A method of bone cutting depth control for surgical robot based on acoustic signals. *Robot.* 2021;43:101–11.

- 38.** Xia G, Jiang Z, Zhang J, Wang R, Dai Y. Sound pressure signal-based bone cutting depth control in robotic vertebral lamina milling. *IEEE Sens J.* 2022;22:10708–18.
- 39.** Xia G, Zhang L, Dai Y, Xue Y, Zhang J. Vertebral lamina state estimation in robotic bone milling process via vibration signals fusion. *IEEE Trans Instrum Meas.* 2022;71:1–11.

- 40.** Xia GM, Yao B, Dai Y, Zhang JX. Cutting depth compensation based on milling acoustic signal for robotic-assisted laminectomy. 2021 IEEE International Conference on Robotics and Automation (ICRA). Xi'an, China: IEEE Conference; 2021. p. 12464–9. <https://doi.org/10.1109/ICRA48506.2021.9561427>